

**Active seismotectonic deformation in front of the Dolomites Indenter, Eastern Alps**

F. Reiter<sup>1</sup>, C. Freudenthaler<sup>2</sup>, H. Hausmann<sup>2</sup>, H. Ortner<sup>1</sup>, W. Lenhardt<sup>2</sup>, and R. Brandner<sup>1</sup>

<sup>1</sup>Institute for Geology, University of Innsbruck, Innsbruck, Austria

<sup>2</sup>Zentralanstalt für Meteorologie und Geodynamik, Vienna, Austria

**Contents of this file**

Figure S1  
Figure S2  
Table S1  
Figure S3  
Figure S4  
Figure S5  
Figure S6  
Figure S7  
Figure S8  
Table S2

**Additional Supporting Information (Files uploaded separately)**

Dataset S1: Catalogue of Fault Plane Solutions of Western Austria and adjacent Regions.  
Dataset S2: Earthquake catalog used.  
Dataset S3: List of earthquake stations.  
Dataset S4: List of relocation data.  
Dataset S5: 1-D velocity model data.  
Dataset S6: Basic data for all focal mechanisms.  
Dataset S7: Additional data for newly calculated fault plane solutions.  
Dataset S8: Results of stress and strain calculations.

## Introduction

The supporting information starts with Figure S1 with lower hemisphere plots to illustrate the focal mechanism calculations. Additionally, we list all calculated and published focal mechanisms and waveform inversions in Table S1. Figure S1 and Table S1 support chapter 6.1. (Results of the focal mechanism calculations).

Figure S2 supports Figure 4 in chapter 6.1 and explains the lower hemisphere diagrams used in Figure 4 in more detail than in the main publication

Figures S3 to S7 are more detailed maps of the seismotectonic domains we found and support Figure 4 and chapter 6.1.

Figure S8 illustrates and lists the results of the stress/strain calculation with the NDA method (chapter 6.2).

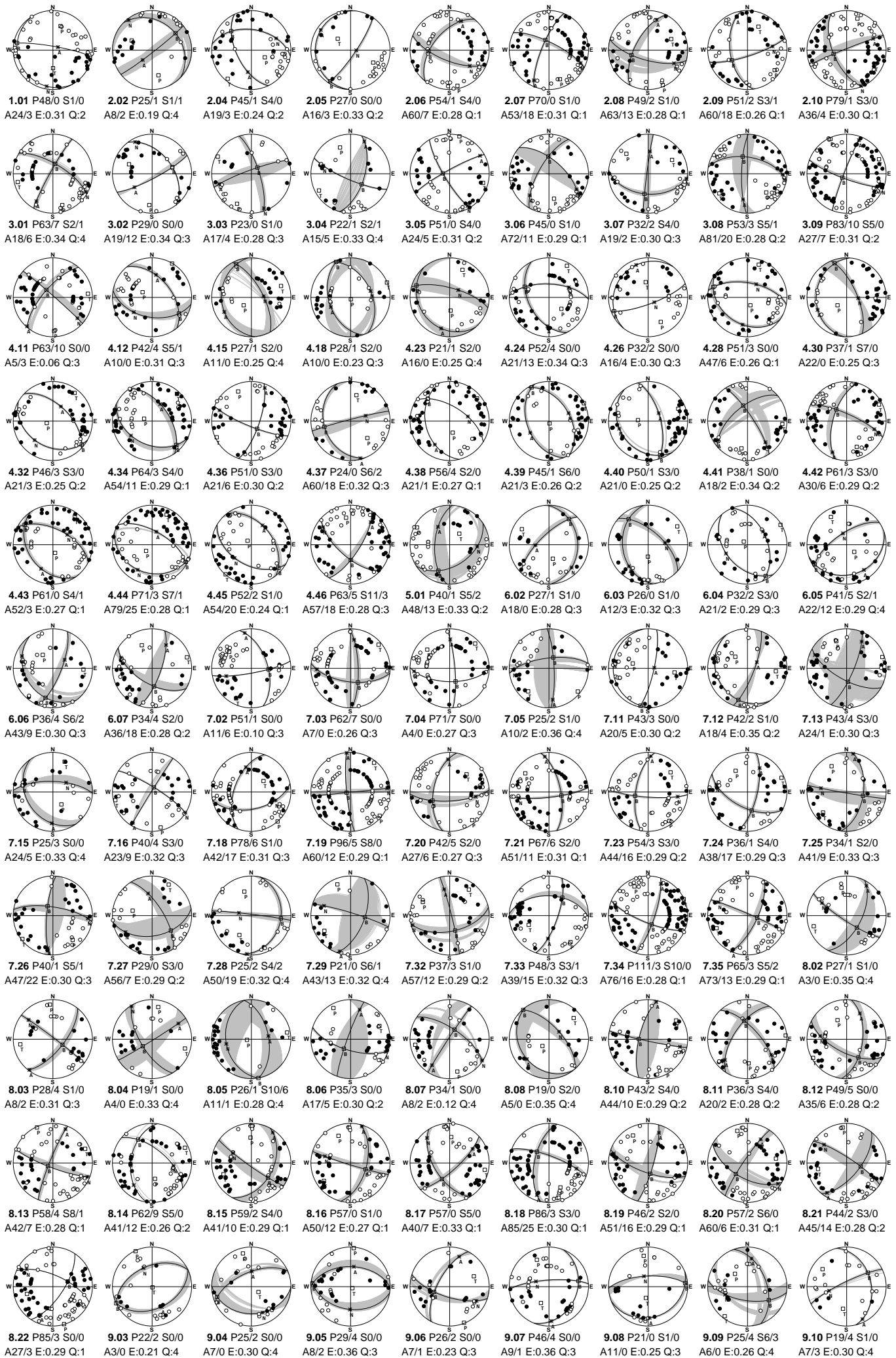
Table S2 lists the numerical results of the stress/strain calculations with the SI (Vavryčuk, 2014), FMSI (Gephart, 1990) and NDA methods (Spang, 1972).

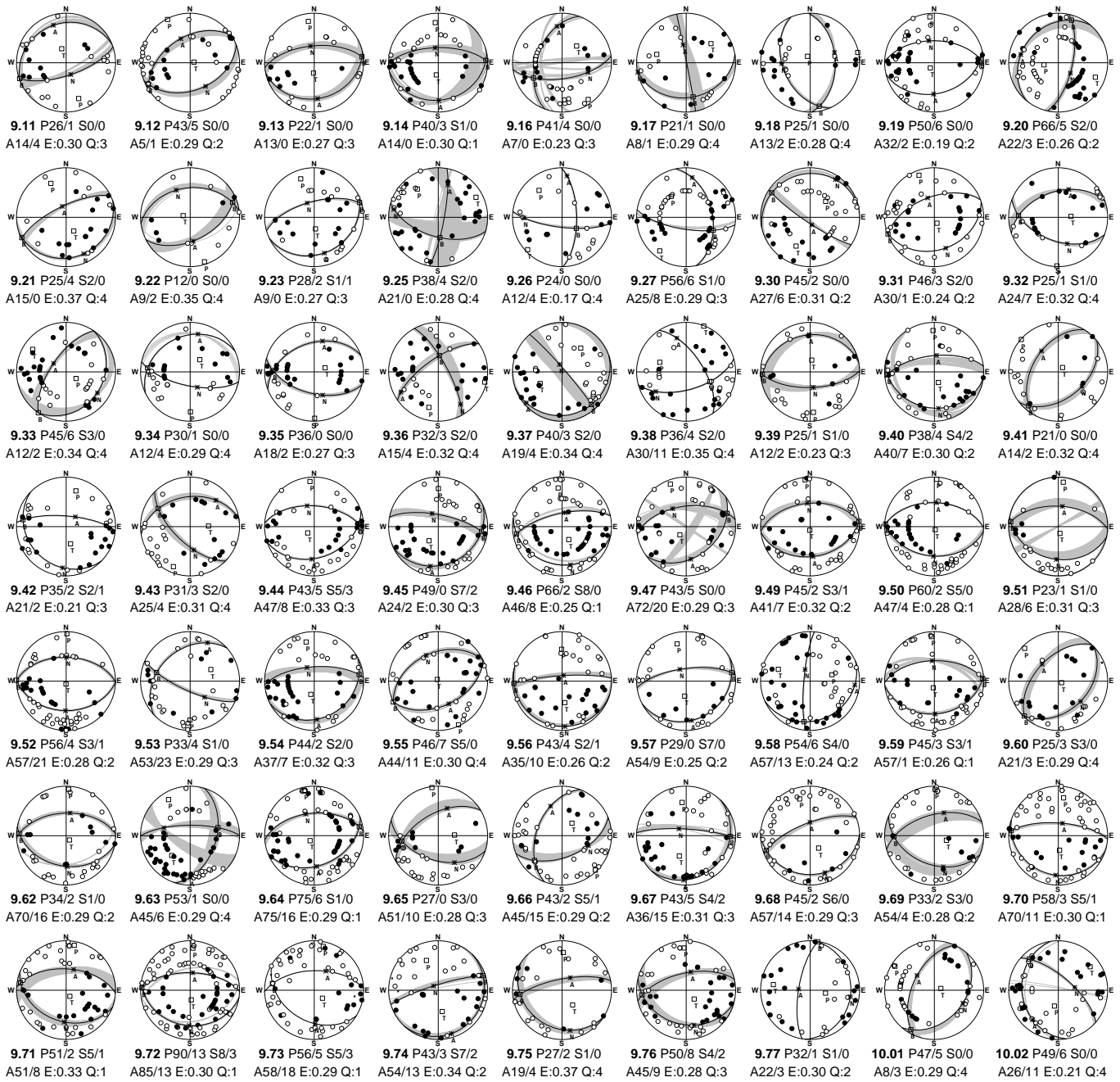
The digital datasets S1-S8 contain a catalogue of all calculated or recalculated focal mechanisms listed and shown in the main publication and numerical values of the fault plane solutions and stress calculations as xlsx or txt tables.

Previously non-public waveform data from network OE and the software used for calculation are available in online repositories (see link on Tectonics article web page).

For references, see main publication.

**Figure S1.** (following two pages) Fault plane solutions calculated for this study. The lower hemisphere equal area plots show compressive P-wave first onsets as white dots and dilatational as black ones. The set of valid solutions calculated in one-degree steps from p-wave first onsets is shown as a cloud of grey great circles. Additionally, SV and SH primary onsets and S/P amplitude ratios were used to narrow and prove the set of valid solutions and to select one, most likely pair of nodal planes (black great circles). P, B and T in the diagram denominate the principal stress axes, A and N the slip lineation on the main and auxiliary nodal planes (see Table S1 for numeric values). The text below the diagrams lists the seismotectonic domain and ID of the event (see main text for details, events are in chronologic order for each domain), the number





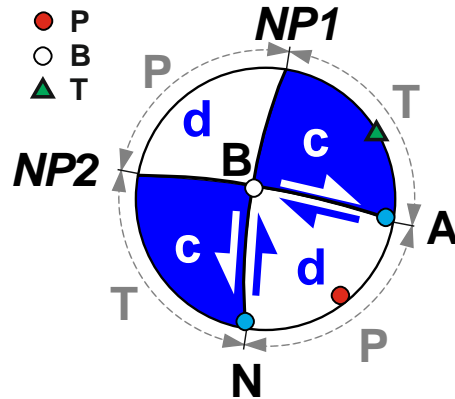


**Figure S2.** The two nodal planes, drawn as great circles on the lower hemisphere (NP1, NP2) divide the diagram area into four areas (dihedra). Dilatational (d) P-wave arrivals are drawn with their azimuth event-station and takeoff angle and plot into the white dihedra, compressive (c) P-wave arrivals plot into the colored dihedra. The fault slip vectors N and A are commonly not drawn and plot on the nodal planes,  $90^\circ$  away from their intersection line which is the position of the intermediate stress axis (B). In the example shown here, NP1 is a sinistral strike-slip fault, NP2 its conjugate counterpart. Both faults produce the same P- and S-wave arrival pattern. Note that the location of the P- and T-axes is not straightforward. If we assume fault reactivation and we do not know which of the two nodal planes is the actual fault, any position of P/T in the dilatational/compressional dihedra would be valid (McKenzie, 1969).

**Table S1.** (following three pages) Numerical details of focal mechanisms from the area shown in Figure 4. Events are ordered by seismotectonic domains (see main text for details). Within each domain, events are sorted chronologically in ascending order (UTC). Lat, Lon, z: hypocentral coordinates; Str (strike), Dip, Rake: orientation of the nodal and auxiliary planes; Azi, Pl: orientation of the P- and T-axes; Class: Fault classification after Johnston et al. (1994), using FMC software (Álvarez-Gómez, 2014): N normal, R reverse, SS strike-slip and combinations in between these end members; Type: Calculation Type: FPS fault plane solution, FWI full waveform inversion; References: 1. new, previously unpublished focal mechanism (this publication); 2. Viganò et al. (2008); 3. Using data from Kraft (1999); 4. Pondrelli et al. (2004); 5. Slejko et al. (1989); Slejko and Rebez (1988); 6. Slejko et al. (1989); 7. Reiter et al. (2005); 8. Roth et al. (1992); 9. Modified by Kastrup et al. (2004); 10. Marschall et al. (2013); 11. Pondrelli et al. (2002); 12. Schweizerischer Erdbebendienst (2017); 13. Deichmann et al. (2004); 14. Baer et al. (2007); 15. Deichmann et al. (2010); 16. Deichmann et al. (2012); 17. Diehl et al. (2013); 18. Istituto Nazionale di Geofisica e Vulcanologia (2017); 19. Bernardi et al. (2005); 20. Braunmiller (2002); 21. Baer et al. (2001); 22. Deichmann et al. (2006); 23. Diehl et al. (2014); 24. Deichmann et al. (2011); 25. Saint Louis University Earthquake Center (2017); 26. Deichmann et al. (2002); 27. Baer et al. (2005); 51. Focal mechanism changed/recalculated with additional data; 52. Fault plane solution calculated using digital waveform data from Diehl et al. (2009); 53. Using relocated coordinates from Viganò et al. (2015); 54. As before, z adjusted to lower error limit given in their paper based on macroseismic evidence and other published localizations cited there. 55. Using waveform data from the AlpArray temporary Network (AlpArray Working Group, 2015).









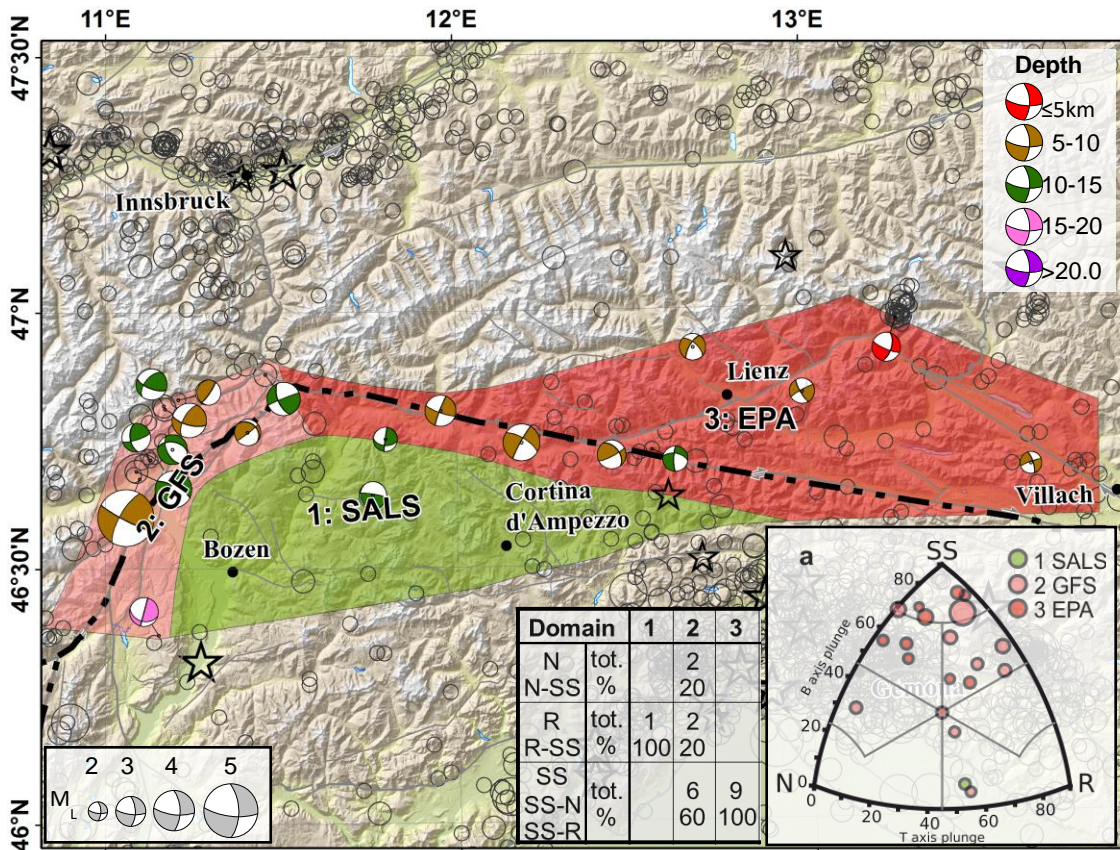


**Figure S3.** Seismicity and focal mechanisms in domains 1, 2, 3: While the interior of the Dolomites Indenter reveals a very low seismicity, the areas close to the Giudicarie Fault System and the Pustertal-Gailtal fault yielded strike-slip solutions with one plane parallel to general fault trend. Ternary diagram after Álvarez-Gómez, 2014.

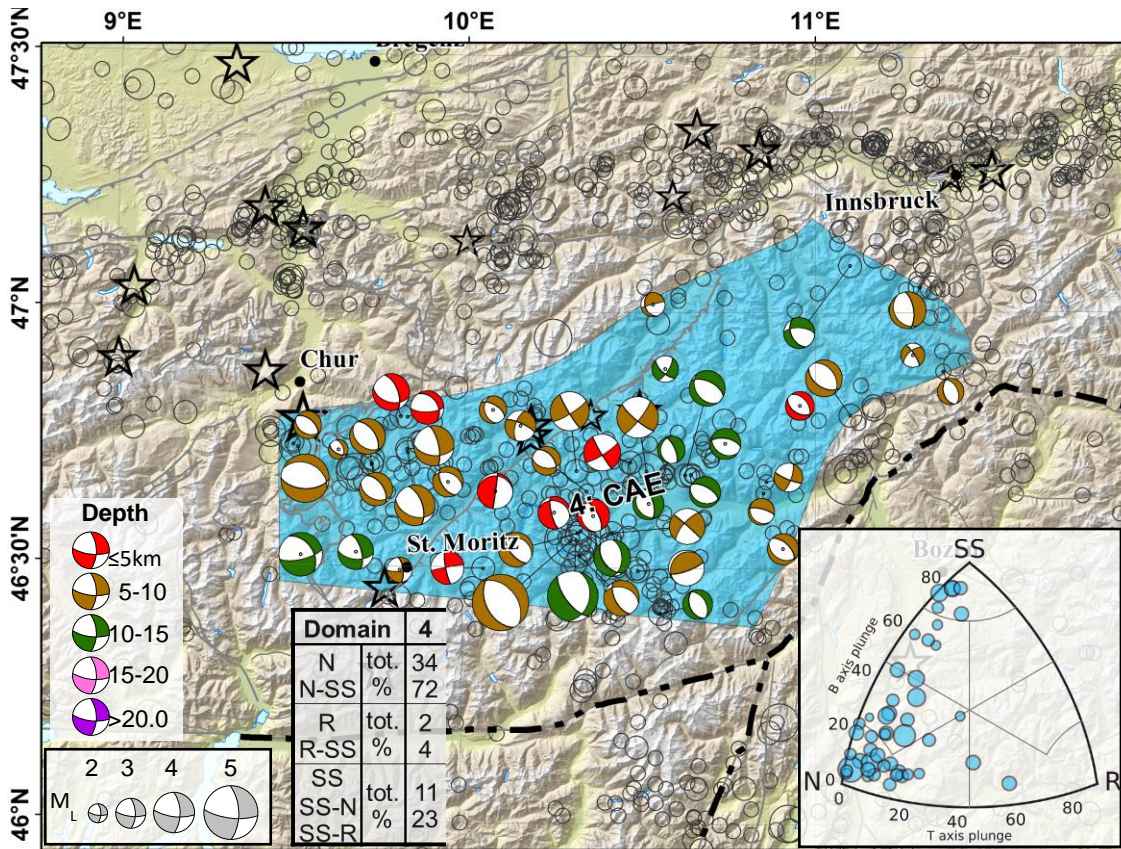


**Figure S4.** Seismicity and focal mechanisms in domain 4: Transtension west of the Dolomites Indenter, Extension northwest of the Indenter corner. Ternary diagram after Álvarez-Gómez, 2014.

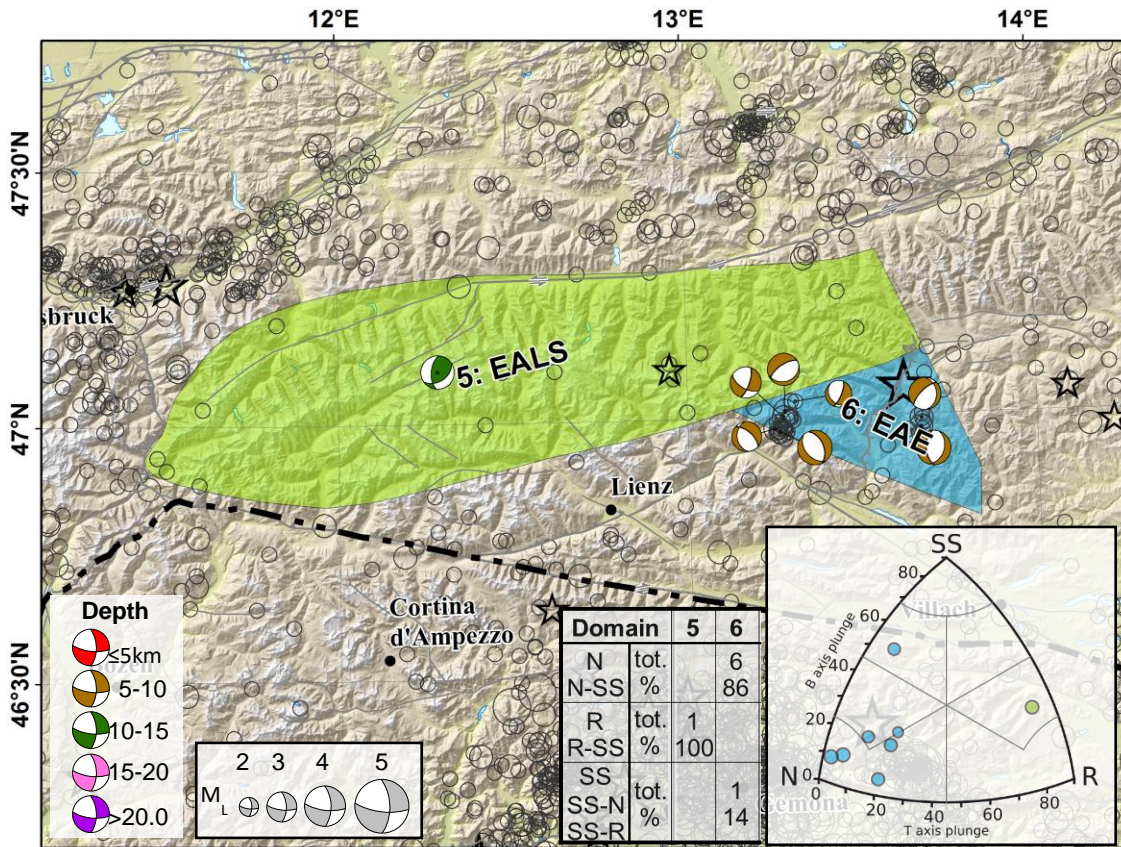


**Figure S5.** Seismicity and focal mechanisms in domains 5 and 6: Domain 5, which partially coincides with the Tauern Window, shows almost aseismic behavior. At the southeastern margin of the Tauern Window ENE to ESE directed extension occurs (domain 6). Ternary diagram after Álvarez-Gómez, 2014.

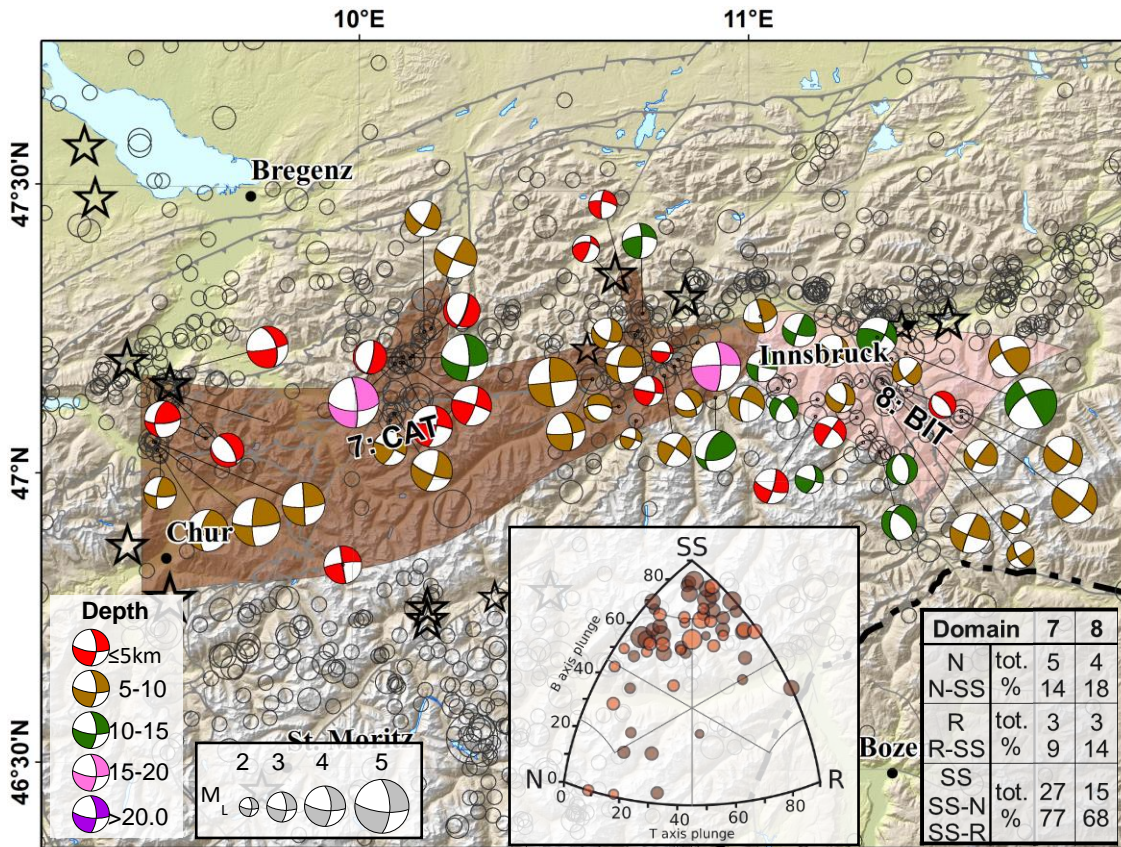


**Figure S6.** Domains 7 (central Alpine transition domain) and 8 (Brenner-Inntal transfer zone). Both domains are dominated by strike-slip faulting, but slightly different orientations of the nodal planes. In domain 7 N-S and E-W striking nodal planes prevail, while domain 8 show mainly NE-SW and NW-SE striking planes. Additionally, orogen-parallel extension is common in domain 8 and rare in domain 7. Ternary diagram after Álvarez-Gómez, 2014.

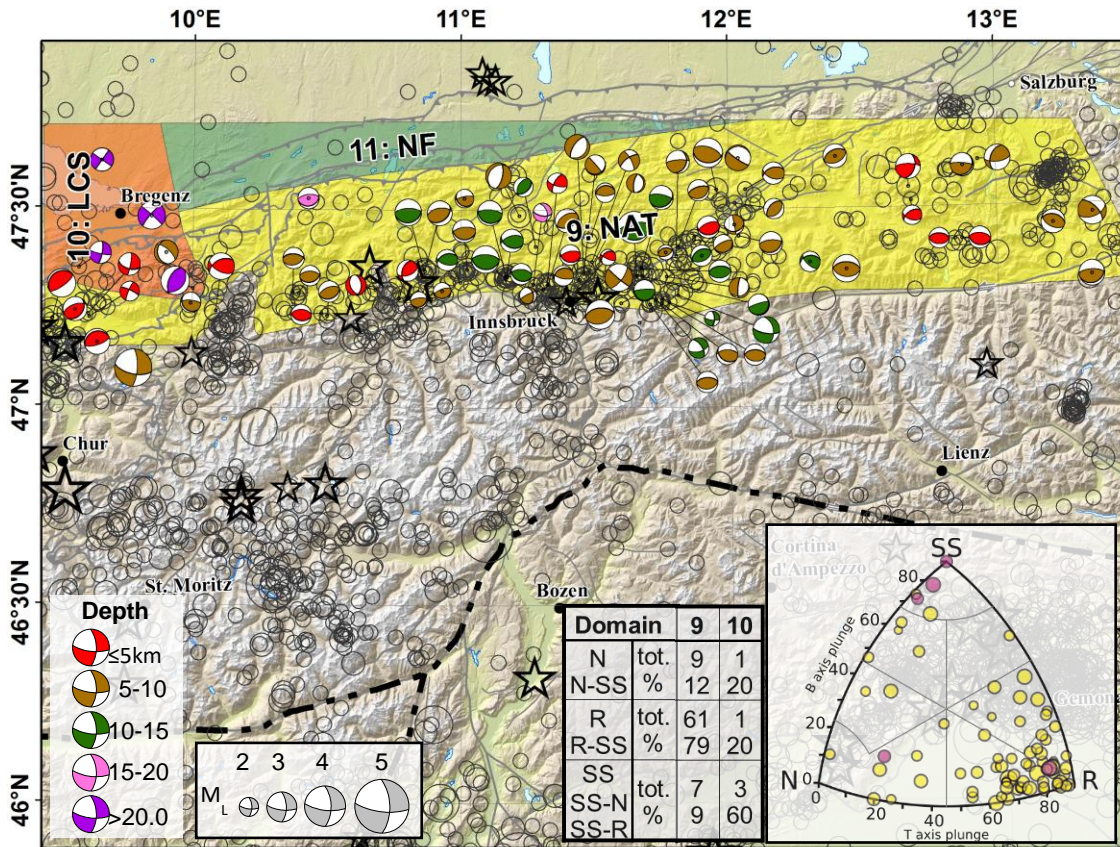
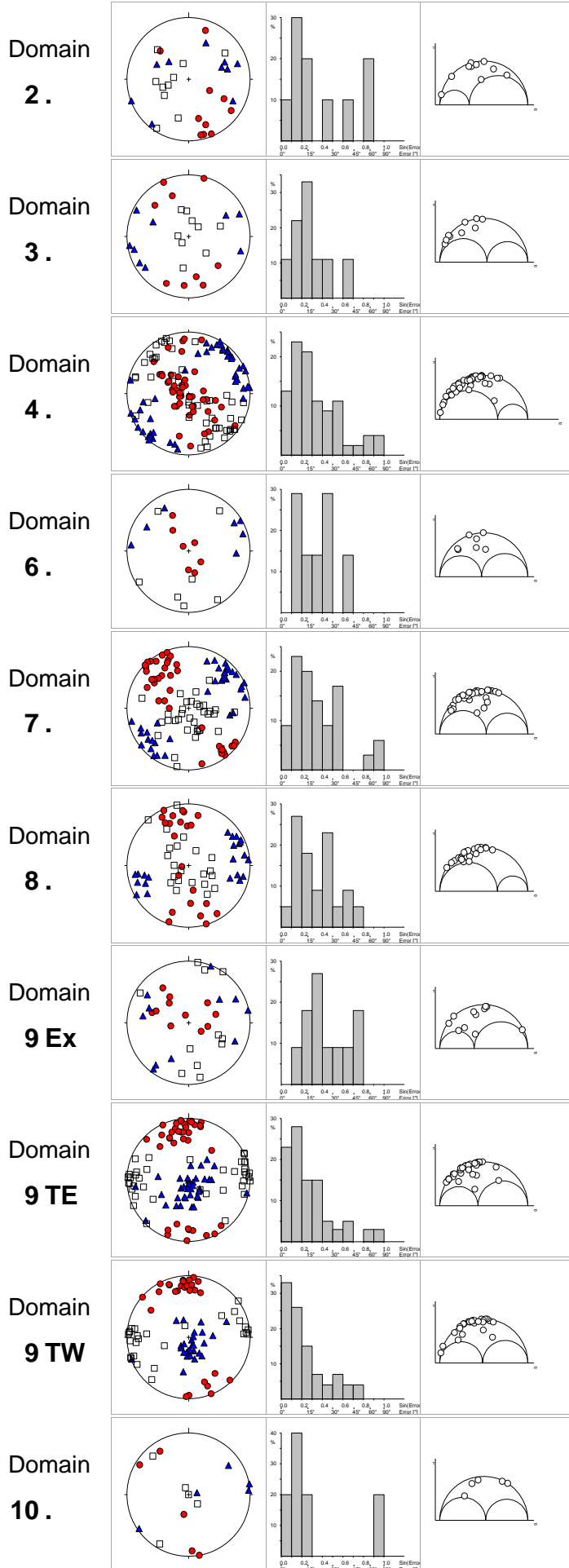


**Figure S7.** Domains 9 (north Alpine thrust domain), 10 (zone of lower crustal seismicity) and 11 (northern foreland). Domain 9 shows majorly thrusting, with occasional strike-slip activity south of the Lower Inn Valley and two spots of orogen-parallel extension. Domain 10 shows prevalingly strike-slip events of NE-SW and NW-SE trend and one thrust. Some of the events (shown in purple) occurred in the lower European crust. The northern foreland (11) is characterized by a very low seismicity. We could not obtain a focal mechanism. Ternary diagram after Álvarez-Gómez, 2014.

**Figure S8 (following page).** Graphical representation of the stress calculations obtained from the NDA method {Spang, 1972 #153}. a. Lower hemisphere Plot of the P-, B- and T-axes. b. Error histogram. Error-axis: angular intervals, calculated as the difference between the observed and the calculated lineation for the given orientation of the principal strain axes. %-axis: Relative number of solutions which fall into the defined angular error interval. c. Normalized Mohr circle. Numerical values: nData: number of input mechanisms;  $\theta$ : angle between the fault slip and the maximum principal strain axis (equivalent to  $\alpha$  in the SI calculation); strain rate: equivalent to the stress rate in the SI calculation,  $\lambda$ ...orientation of the principal strain axes. Strain reg.: Strain regime, equivalent to stress regime, see main publication for details.

a. PBT-and Strain axes b. Err. Histogram. c. Norm. Mohr Circ.



Azim Plunge

nData	10	Lambda 1	160	18
Theta	45	Lambda 2	294	65
Strain Rate	0,3338	Lambda 3	064	17
neg. sense for	1	dataset(s):		

2.10

Strain reg. transpression

nData	9	Lambda 1	169	12
Theta	45	Lambda 2	350	78
Strain Rate	0,5362	Lambda 3	259	00
neg. sense for	0	dataset(s):		

err=40° for 3.02

Strain reg. strike-slip

nData	47	Lambda 1	259	86
Theta	45	Lambda 2	143	02
Strain Rate	0,6581	Lambda 3	053	04
neg. sense for	2	dataset(s):		

4.01;4.26

Strain reg. transtension

nData	7	Lambda 1	189	83
Theta	45	Lambda 2	350	06
Strain Rate	0,4754	Lambda 3	080	02
neg. sense for	0	dataset(s):		

err=44° for 6.05

Strain reg. extension

nData	35	Lambda 1	321	13
Theta	45	Lambda 2	162	76
Strain Rate	0,5287	Lambda 3	052	05
neg. sense for	0	dataset(s):		

err=69° for 7.11;7.15 err=59° for 7.28

Strain reg. strike-slip

nData	22	Lambda 1	346	10
Theta	45	Lambda 2	187	80
Strain Rate	0,6544	Lambda 3	077	04
neg. sense for	0	dataset(s):		

err=47° for 8.08

Strain reg. transtension

nData	11	Lambda 1	340	76
Theta	45	Lambda 2	139	13
Strain Rate	0,3911	Lambda 3	230	05
neg. sense for	0	dataset(s):		

err=45° for 9.20

Strain reg. extension - radial ext.

nData	39	Lambda 1	351	10
Theta	45	Lambda 2	261	02
Strain Rate	0,4343	Lambda 3	163	80
neg. sense for	0	dataset(s):		

err=55° for 9.26; 69° for 9.36

Strain reg. thrust

nData	27	Lambda 1	346	10
Theta	45	Lambda 2	256	01
Strain Rate	0,4865	Lambda 3	160	80
neg. sense for	0	dataset(s):		

err=53° for 9.02

Strain reg. thrust

nData	5	Lambda 1	159	02
Theta	45	Lambda 2	257	73
Strain Rate	0,5223	Lambda 3	068	16
neg. sense for	0	dataset(s):		

err=71° for 9.01

Strain reg. strike-slip

Domain	Azimuth of $\sigma_H/\lambda_H$ [°]				Stress/strain ratio $\phi_\sigma/\phi_\lambda$				Average rotational misfit [°]
	SI	FMSI	NDA	Max $\Delta$	SI	FMSI	NDA	Max $\Delta$	FMSI
<b>2. GFS</b>	161	156	158	05	0.44	0.35	0.33	0.11	5.7
<b>3. EPA</b>	175	158	169	17	0.32	0.80	0.54	0.48	3.5
<b>4. CAE</b>	144	152	143	09	0.70	0.55	0.66	0.15	5.7
<b>6. EAE</b>	166	166	170	04	0.26	0.30	0.48	0.21	3.1
<b>7. CAT</b>	144	134	141	10	0.41	0.45	0.53	0.12	5.9
<b>8. BIT</b>	165	155	166	12	0.53	0.40	0.65	0.25	5.6
<b>9 NA-Ex</b>	139	118	142	24	0.19	0.50	0.39	0.31	6.1
<b>9 NA-TE</b>	174	149	172	27	0.12	0.75	0.43	0.63	5.5
<b>9 NA-TW</b>	168	163	166	05	0.31	0.40	0.49	0.17	4.8
<b>10. LCS</b>	150	136	158	23	0.37	0.85	0.52	0.48	1.5

**Table S2.** Numerical results of the stress/strain calculations with the SI (Vavryčuk, 2014), FMSI (Gephart, 1990) and NDA methods (Spang, 1972). The first row denominates the stress subdomain, followed by the azimuths of maximum horizontal stress/strain  $\sigma_H/\lambda_H$  calculated by the three different methods and the maximum difference between the results ( $\Delta$ ). Next, we compare the stress/strain ratios  $\phi_\sigma/\phi_\lambda$  and list their maximum difference. In the last row, we show the angular rotational misfit of the nodal plane dataset.

**Data Set S1. Catalogue of fault plane solutions of western Austria and adjacent regions:**  
2017TC004867\_DS01\_Datasheets\_05.pdf

Contains input parameters for calculations, numeric and graphic results, focal mechanism classification scheme, pick classification scheme, velocity model details.

**Data Set S2. Earthquake catalog of western Austria and adjacent regions:**  
2017TC004867\_DS02\_Earthquake\_Catalog.xlsx

We compiled the earthquake catalog used for this study from several sources. The data are attached in xlsx format. For contributing agencies, see acknowledgements of main text. Published events referred to are listed in the reference section of the main text.

**Data Set S3. Station list:** 2017TC004867\_DS03\_StationList.xlsx

Station list in xlsx format.

**Data Set S4. Relocation data:** 2017TC004867\_DS04\_RelocationData.xlsx.

Relocation data in xlsx format.

**Data Set S5. Velocity model:** 2017TC004867\_DS05\_TauP\_VelMod.

1D velocity model used for angular calculations in TauP format (Crotwell and Owens, 2016).

**Data Set S6. Basic data for all focal mechanisms:**

2017TC004867\_DS06\_FocalMechanisms.xlsx.

Table S1 of supporting information in xlsx format plus the active focal plane as determined by the SI calculation.

**Data Set S7. Additional data for fault plane solutions calculated for this study:**

2017TC004867\_DS07\_FPS\_Details.xlsx.

Numerical data shown in Figure S1 of supporting information in xlsx format.

**Data Set S8. Results of stress and strain calculations:**

2017TC004867\_DS08\_Stress\_Calculations.xlsx

Numerical data shown in Figure 6 of main publication in xlsx format. Additionally, also numerical results from other calculation methods not shown in Figure 6 and from neighboring areas with published results of stress calculations shown in Figure 7.